



BNL-212226-2019-JAAM

# A new luminescence lifetime macro-imager based on Tpx3Cam optical camera

R. Sen, A. Nomerotski

To be published in "Biomedical Optics Express"

November 2019

Physics Department  
**Brookhaven National Laboratory**

**U.S. Department of Energy**  
USDOE Office of Science (SC), High Energy Physics (HEP) (SC-25)

Notice: This manuscript has been authored by employees of Brookhaven Science Associates, LLC under Contract No. DE-SC0012704 with the U.S. Department of Energy. The publisher by accepting the manuscript for publication acknowledges that the United States Government retains a non-exclusive, paid-up, irrevocable, world-wide license to publish or reproduce the published form of this manuscript, or allow others to do so, for United States Government purposes.

## **DISCLAIMER**

This report was prepared as an account of work sponsored by an agency of the United States Government. Neither the United States Government nor any agency thereof, nor any of their employees, nor any of their contractors, subcontractors, or their employees, makes any warranty, express or implied, or assumes any legal liability or responsibility for the accuracy, completeness, or any third party's use or the results of such use of any information, apparatus, product, or process disclosed, or represents that its use would not infringe privately owned rights. Reference herein to any specific commercial product, process, or service by trade name, trademark, manufacturer, or otherwise, does not necessarily constitute or imply its endorsement, recommendation, or favoring by the United States Government or any agency thereof or its contractors or subcontractors. The views and opinions of authors expressed herein do not necessarily state or reflect those of the United States Government or any agency thereof.

# A new luminescence lifetime macro-imager based on Tpx3Cam optical camera

Rajannya Sen<sup>1†</sup>, Liisa M. Hirvonen<sup>2†</sup>, Alexander V. Zhdanov<sup>1</sup>, Peter Svihra<sup>3,4</sup>, Stefan Andersson-Engels<sup>5</sup>, Andrei Nomerotski<sup>6\*</sup>, Dmitri B. Papkovsky<sup>1,5\*</sup>

<sup>1</sup>School of Biochemistry and Cell Biology, University College Cork, Cork, Ireland, <sup>2</sup>Randall Centre for Cell and Molecular Biophysics, King's College London, Guy's Campus, London SE1 1UL, United Kingdom,

<sup>3</sup>Department of Physics, Faculty of Nuclear Sciences and Physical Engineering, Czech Technical University, Prague 115 19, Czech Republic; <sup>4</sup>Department of Physics and Astronomy, School of Natural Sciences, The University of Manchester, Manchester M139PL, United Kingdom; <sup>5</sup>Irish Photonics Integration Centre, Tyndall National Institute, Cork, Ireland; <sup>6</sup>Physics Department, Brookhaven National Laboratory, Upton, New York, 11973 USA.

**KEYWORDS:** *Phosphorescence Lifetime Imaging (PLIM), Fluorescence Lifetime Imaging (FLIM), Time Correlated Single Photon Counting (TCSPC), Macroscopic imaging, Oxygen sensing and imaging, Tpx3Cam*

---

**ABSTRACT:** Properties of a novel ultra-fast optical imager, Tpx3Cam, were investigated for macroscopic wide-field phosphorescent lifetime imaging (PLIM) applications. The camera is based on a novel optical sensor and Timepix3 readout chip with time resolution of 1.6 ns, recording of photon arrival time and time over threshold for each pixel, and readout rate of 80 megapixels per second. In this study, we coupled the camera to an image intensifier, a 760 nm emission filter and a 50 mm lens, and with a super-bright 625nm LED providing pulsed excitation of a 18x18mm sample area. The resulting macro-imager with compact and rigid optical alignment of its main components was characterised using planar phosphorescent O<sub>2</sub> sensors and a resolution plate mask. Several acquisition and image processing algorithms were evaluated to optimise the system resolution and performance for the wide-field PLIM, followed by imaging a variety of phosphorescent samples. The new PLIM system looks promising, particularly for phosphorescence lifetime-based imaging of O<sub>2</sub> in various chemical and biological samples.

---

## 1. INTRODUCTION

Fluorescence Lifetime IMaging (FLIM) is gaining popularity in the biological and medical research<sup>1-3</sup> since FLIM measurements are less affected by the factors influencing fluorescence intensity such as probe concentration, photobleaching, excitation intensity, optical alignment, scattering and autofluorescence. As a result, FLIM can provide quantitative, calibration-free imaging readouts and minimise measurement artefacts. Nanosecond FLIM with short-lived fluors is actively used, e.g. in molecule interaction studies by FLIM-FRET, in the analysis of cell autofluorescence, pH, Ca<sup>2+</sup>, glucose dynamics and other parameters<sup>4-9</sup>. Phosphorescence lifetime imaging (PLIM) is also very attractive but less common due to the low availability of corresponding equipment and biomaterials. PLIM is mainly applied in quenched-phosphorescence imaging of O<sub>2</sub> in various samples and in luminescent barometry<sup>10-13</sup>, using long-decay photoluminescent materials based on transition metal complexes and

metalloporphyrins, with lifetimes in the microsecond time range.

The classical technique for recording fluorescence lifetimes is Time Correlated Single Photon Counting (TCSPC), in which a pulsed excitation laser is coupled with a single photon counting detector, which uses fast timing electronics to detect the emitted photons and then extract the characteristics of emission decay. A short excitation pulse is sent to the sample and timing electronics to start the timer, and a stop signal is generated when the system detects the first photon. After multiple excitation and recording events, an emission decay profile is obtained. For FLIM, this TCSPC technique is combined with a pixel-by-pixel scanning of the sample. For thick samples the imaging depth and contrast can be improved by using a confocal laser scanning setup with pinhole optics which prevents unfocused light reaching the detector, or two-photon excitation. Laser scanning TCSPC-FLIM has advanced in recent years in its optoelectronic components, sensitivity,

excitation sources and emission range, and has been implemented in clinical applications, including dermatology<sup>14</sup>, ophthalmology<sup>15</sup>, and cancer<sup>16</sup>. However, pixel-by-pixel scanning leads to slow image acquisition times<sup>17-19</sup>, particularly for PLIM applications where long pixel dwell times are required to record the long-lived phosphorescence.

Wide-field FLIM imaging, where the whole field of view is imaged simultaneously onto a camera, is possible with gating and frequency-domain methods, however these methods are not single photon sensitive. One technique relies on a gated CCD camera coupled to a photon counting image intensifier such as the microchannel plate (MCP). The gated image intensifier provides time resolution as fluorescence decay is calculated from a set of intensity frames acquired with different delays after the excitation pulse. This, however, leads to the loss of photons outside the MCP gate and is influenced by sample photobleaching or any other time-dependent effects. In frequency domain FLIM, on the other hand, a gain modulated image intensifier and CCD detector are used to record the amplitude difference and phase delay between the excitation and the emission signal. The phase shift obtained is related to the fluorescent lifetime of the fluorophore. Although this technique is advantageous for real time monitoring, it usually requires high signals, and is influenced by scattered light, photobleaching and autofluorescence<sup>17,20,21</sup>.

Fast wide-field FLIM with single photon sensitivity has been demonstrated with a photon counting image intensifier and a CMOS camera. The location and arrival time of the photons in each frame were extracted with software by fitting an exponential decay function fitted to the arrival time histogram in each pixel to obtain the lifetime image<sup>22</sup>. The time resolution in this case is limited by the camera frame rate. To improve time resolution, this technique was extended by exploiting the invariant decay of the image intensifier's phosphor screen to determine the arrival time of the photons with sub-exposure time accuracy. The detection of the position of the photon by centroiding technique along with single photon sensitivity provide excellent spatial resolution, a time resolution of 40 ns and a framerate of 250 kHz for the image size of 80x128 pixels<sup>23,24</sup>.

Solid-state single photon detectors were recently introduced to wide-field TCSPC-FLIM. Here, single photon avalanche photodiodes (SPADs) were integrated into compact imaging array detectors. A SPAD is a p-n junction diode that is biased above the breakdown voltage, so that a single photon can generate an electron-hole pair leading to an avalanche signal multiplication. SPAD array sensors have single photon sensitivity, picosecond time resolution, and each pixel can independently perform TCSPC. While being a very promising technology due to excellent time resolution, current SPAD imagers still require improvements of the SPAD photon detection efficiency, array density and dark count rate<sup>20,25</sup>.

Another technology with parallel photon detection in each pixel was implemented in the TimepixCam

camera<sup>26,27</sup>. The camera combined the Timepix chip<sup>28</sup> with 256x256 pixels and an optimized optical sensor in a novel time-stamping optical imager. The silicon sensor has a thin entrance window and anti-reflective coating with enhanced QE in the wavelength range 400-1000 nm<sup>29</sup>. Intensified version of the camera had single photon counting ability detecting the photon arrival times in each pixel. This camera has been demonstrated in PLIM of 200  $\mu$ m polystyrene beads stained with a long-decay time fluorescent iridium complex achieving 15 ns timing resolution and ns-scale lifetime resolution<sup>30</sup>. The system operated in the visible range and microscopic format, which are not quite optimal for biomedical applications. The main limitation of the camera was a slow readout, which allowed only a 10Hz excitation frequency leading to very long image acquisition times.

Recently, the next generation camera, Tpx3Cam, has become available, based on the same optical sensor as above and Timepix3 readout chip<sup>31</sup>. Timepix3 improves the camera time resolution to 1.6 ns. It also has fast readout rate of 80 Mpixel/s. The time over threshold (TOT) and time of arrival (TOA) of each pixel that exceed a pre-set threshold are measured and stored by the internal pixel circuitry. The pixel light detection threshold (non-intensified version) corresponds to about 600 photons depending on the wavelength. The deadtime of individual pixels to process and store the information after they were hit is about 475 ns plus the corresponding TOT.

The camera readout is based on the SPIDR system<sup>32</sup> and is data-driven so only the pixels containing the non-zero information are transferred from Timepix3 to SPIDR and read out to the outside world via a 1Gbps or 10Gbps links. The SPIDR also has an internal TDC which is able to time-stamp incoming digital pulses with 0.26 ns precision synchronously with the Timepix3 hits. This feature is useful to provide an external time reference and sometimes is referred to as the 'trigger' input though it is completely independent from the Timepix3 operations. To date, the camera has been used in several applications, including imaging mass spectrometry, quantum imaging and optical readout of a liquid argon time-projection chamber<sup>33-36</sup>.

For TCSPC FLIM applications, where the single photon sensitivity is essential, Tpx3Cam must be coupled to an image intensifier, a vacuum device with a photocathode, which converts incident photons into photoelectrons. The electrons are then multiplied by an MCP and directed on to the P47 scintillating screen. The screen converts these electrons into a fast flash of photons focussing it onto the optical sensor inside Tpx3Cam and generating signals in the respective pixel front-end electronics.

So far, FLIM/PLIM has been used mainly in microscopic imaging, while macroscopic applications are less common. For microscopy, cameras with relatively low spatial resolution and long acquisition times were used<sup>37</sup>. The DSC-120 MACRO FLIM/PLIM confocal imager offered by Becker and Hickl (Germany)<sup>37</sup> can image objects to a size of 12

mm with high resolution, but it is still slow due to its scanning mode. On the other hand, macroscopic luminescence imaging is in demand for biomedical and life sciences, where currently the intensity-based imagers are mostly used<sup>38</sup> which lack accurate and quantitative optical readout.

In this work, we constructed a new imager based on Tpx3Cam that can image large objects (currently 18x18 mm, can be increased) in the microsecond PLIM mode. The Timepix camera has previously been used in PLIM applications<sup>30</sup>, but in a traditional stationary alignment of discrete elements on the optical bench and also with severe rate limitations. Here, we used the Cricket® adaptor<sup>39</sup> with an image intensifier, a 760 nm emission filter and 50 mm lens, thus retaining compact size and flexibility of the imager, which can be manipulated as a single unit almost like a standard photographic camera and moved to different locations. Key parameters of the imager were tested and optimised to obtain fast and accurate lifetime determination and high spatial resolution at the output. Finally, we demonstrated the system in quenched-phosphorescence sensing and imaging of O<sub>2</sub> in chemical and biological samples.

## 2. METHODS

### 2.1 MACRO IMAGER SETUP

The Tpx3Cam (Amsterdam Scientific Instruments) was attached via its C-mount connector to the Cricket® adaptor (Photonis), which housed an image intensifier, a 25 mm 760±50 nm emission filter (Edmund Optics) and which on the other side was connected to the Navitar NMV-50M11" 50 mm lens via another C-mount connector. Figure 1 shows the experimental setup and, schematically, components of the intensified Tpx3Cam. The Cricket® is a plug-and-play electro-optical adapter, which holds and aligns the key optoelectronic components of the PLIM system, improving the quality of intensified images and providing flexibility, so that it can be rotated 360° and tuned geometrically for analysis of different samples. A super bright red 5mm LED with the central wavelength at 627 nm (12,000 mcd, 8° angle, Parts Express) was used to excite the sample.

The intensifier from Photonis, PP0360EF, had the S25 photocathode with diameter of 18mm, quantum efficiency of about 8% at 780 nm and total dark count rate of 40 kHz at room temperature. The intensifier was connected to a standard power supply (Thundar, 72-10495) with one channel providing the power and the other one regulating the intensifier gain. Two channels of fast pulse generator (Tenma, TGP110) were used to send synchronization pulses to the camera and to pulse the LED. Typically, the synchronization pulse was preceding the LED pulse by 10 μs as illustrated in Figure 2. For the measurements in this work the Tpx3Cam imager was mostly used in the upright orientation as shown in Figure 1. Imaged samples were placed on a Thorlabs stage, which allowed the sample movement in X-Y-Z dimensions and focussing. The distance to object was kept at around 8 cm for best focus. A 525 x 375 x 300

mm black box (Thorlabs, XE25C9/M) protected the system from ambient light minimising spurious background count.

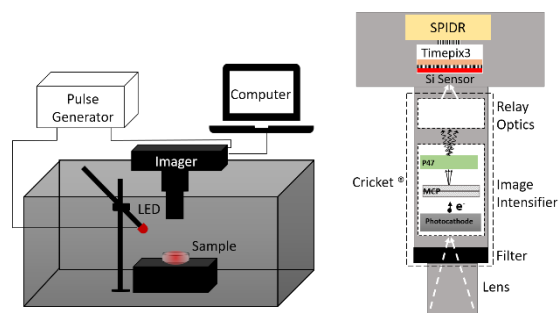


Figure 1. (Left) Experimental setup of the PLIM macro-imager based on Tpx3Cam. (Right) Components of the intensified Tpx3Cam.

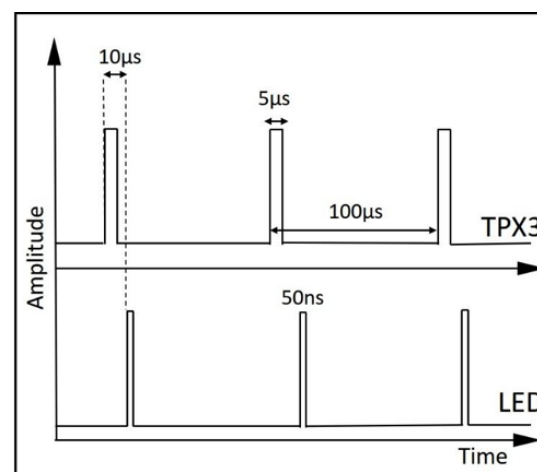


Figure 2. Pulsing scheme of the imager. The LED is pulsed every 100 μs with 50 ns duration of the pulse. Tpx3Cam is provided with a synchronous pulse 10 μs before the LED, which is time-stamped and included into the data stream. The camera records the photon hits for 100 μs until the next LED pulse.

### 2.2 IMAGE ACQUISITION AND DATA PROCESSING

Sophy™ software, provided by Amsterdam Scientific Instruments, was used as an online display for tuning the operational parameters, focussing and alignment. After this a custom-designed software was used to acquire the Tpx3Cam raw data in binary format and to post-process it. The post-processing code time-orders the hit pixels and trigger signals, and provides output in ASCII format listing the following parameters for each hit pixel: excitation trigger time, pixel X and Y coordinates, TOA (time of arrival = pixel time since start of experiment), TOT (time over threshold = amplitude) and (TOA - trigger time) = pixel time since the start of the current excitation period.

The post-processed data was then analysed with a dedicated program written in C-language. Sum images were obtained by including all hit pixels into the final image. For centroided images, clusters of hit pixels having size between 3 and 15 pixels were identified for each excitation period, and the centroid pixel of each cluster was determined from the TOT by center-of-mass centroiding (unless otherwise stated). For the centroided image only this centroided position was recorded for each cluster. The lifetime images were then created by placing all photons into an XYt data cube and writing the data into an .ics image file. A two-exponential function  $I(t) = A_1 \exp(-t/\tau_1) + A_2 \exp(-t/\tau_2)$  was used to fit the phosphorescence decay in each pixel of the image in Tri2 software<sup>40</sup>. The average lifetime  $\bar{t} = (\alpha_1 \tau_1^2 + \alpha_2 \tau_2^2) / (\alpha_1 \tau_1 + \alpha_2 \tau_2)$  obtained from this fit was encoded in a pseudocolor scale (blue for short lifetimes and red for long lifetimes), yielding a phosphorescence lifetime image. A phosphorescence intensity image was obtained by summing all photons together.

### 2.3 SAMPLE PREPARATION

The USAF resolution test target (Thorlabs) was used to determine the spatial resolution of the camera (Figure 3a). To characterize the imager, a planar phosphorescent O<sub>2</sub>-sensor, which comprised a 15 μm thick coating of PtBP dye (Luxcel Biosciences) in RL-100 polymer (Degussa), 1% w/w, deposited on an 80 μm thick polyester film (Mylar, DuPont) by spin-coating<sup>41</sup>. The sensor photograph and its UV-Vis absorption spectrum are shown in Figure 3b, c. Sensor dots, sized 7-10 mm (Figure 3d), were produced by spotting the same sensor cocktail on a microporous PVDF membrane (Millipore). Another planar O<sub>2</sub> sensor containing PtBP and an additional aza-Bodipy dye (4,4-difluoro-1,3,5,7-tetraphenyl-4-bora-3a,4a,8-triaza-s-indacene) with excitation maximum at 650 nm (Figure 3e,f) and fluorescence at around 672 nm<sup>42,43</sup>, was used to measure the instrument response function.

The sample with live mammalian cells comprised a 1.5 mL Eppendorf tube filled with DMEM growth media in which 5x10<sup>6</sup> HCT116 cells (human colon cancer cell line) cultured under standard conditions were precipitated at the bottom of the tube by mild centrifugation at 200 g. A water-soluble phosphorescent probe, NanO2-IR (Luxcel Biosciences), which is also based on RL-100 polymer and PtBP dye<sup>44</sup>, was added to the media at a final concentration of 1 mg/ml, and after a 30 min incubation at 37°C the tube was imaged by Tpx3Cam. The corresponding results are presented in Section 3.4.

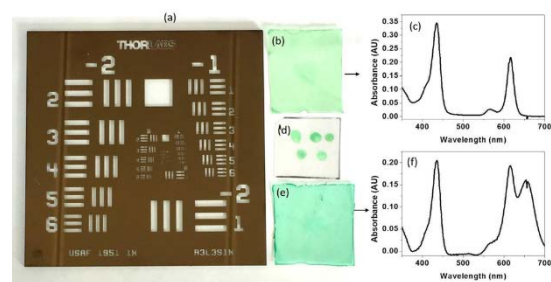


Figure 3. Samples used to characterize the imager: (a) USAF resolution test target; (b) Planar PtBP-RL100 based O<sub>2</sub> sensor film and (c) its absorption spectrum; (d) PtBP-RL100 sensor spots on PVDF membrane, (e) Sensor film with PtBP and aza-Bodipy dyes in RL100, and (f) its absorption spectrum. Spectra were measured on an 8453UV-Visible spectrophotometer (Agilent).

## 3. RESULTS AND DISCUSSION

### 3.1 SINGLE PHOTON EVENTS

The images of single photon events observed with the Tpx3Cam were approximately round, with a typical diameter of ~3 pixels, as shown in Figure 4. As expected, the pixels have higher TOT in the centre of the event (Figure 4a). Figure 4b shows time stamps for photons arriving at random times, where the events are clearly identifiable by their arrival time. However, the events themselves also have a time distribution, where the centre of the photon event with the highest flux has the earliest time stamp, and the time stamps of the surrounding pixels are delayed (Figure 4c-e). This effect is due to the lower flux in these pixels as the corresponding pulses have a slower rise time and, therefore, cross the threshold slightly later, an effect known as “timewalk”<sup>45,46</sup>. As each cluster represents a single photon which has only one arrival time, we have tested the effect of centroiding on the spatial and temporal resolution.

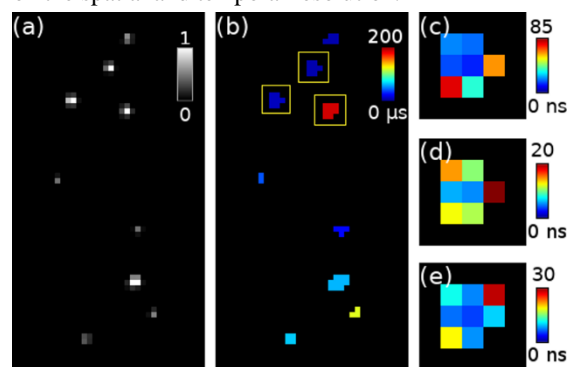


Figure 4. Single photon events detected with the Tpx3Cam setup. (a) TOT, i.e. intensity, (b) arrival time, (c-e) Re-scaled arrival time for individual photon events showing the “timewalk” effect.

### 3.2 SPATIAL RESOLUTION AND COMPARISON OF THE DIFFERENT CENTROIDING METHODS

To measure the spatial resolution of the PLIM system, a 1951 USAF resolution test target (Figure 3a) was placed on top of the planar O<sub>2</sub> sensor foil (Figure 3b) and imaged with Tpx3Cam. LED at 8V power and a pulse width of 500ns was used to excite the sample (Figure 5a). Data was collected for 60 seconds, during which a total of 612,072 “frames” (excitation periods) with 131 million triggered pixels were acquired at a pixel readout rate of 2.2 MHz. In this data, 26 million photon events were found in the size range of 3-15 pixels, with 2.4 million undersize (<3 pixels) and 1.9 million oversize (>15 pixels) events discarded. This corresponds to accepted photon event count rate of ~0.43 MHz.

The data was processed with different centroiding methods to compare their effect on the spatial resolution. Figure 5a shows the whole 17.7 x 17.7 mm field of view (FoV) of the PLIM macro imager system. A noticeable gradient in the intensity is due to the non-uniformity of the illumination system made of a single LED. Figures 5b-e show the central area of the FoV processed with different centroiding methods. As expected, the sum image (Figure 5b), where all hit pixels are summed for the final image, shows worst resolution, since in this case the photon events cover a large area and smear the image. Brightest pixel centroiding (Figure 5c) and timecode centroiding (Figure 5d), where the photon event centre is assigned to the pixel with highest TOT or the earliest timecode, respectively, provided some improvement of resolution. Best resolution was achieved with sub-pixel centroiding (Figure 5e), where each pixel is divided into sub-pixels (here 5x5 sub-pixels) and the photon coordinates are found by centre-of-mass calculation using the TOT information. Figure 5f shows cross-sections of bars indicated in Figure 5e, where the bars are easily resolved with the sub-pixel centroiding method but cannot be resolved in the other images. This centroiding technique provided a resolving power of 12.7 lp/mm with line width 39.4 μm.

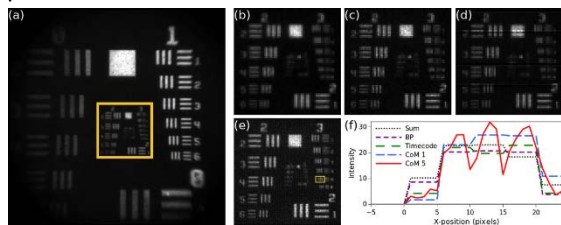


Figure 5. Images of 1951 USAF resolution test target overlaid on top of a phosphorescent O<sub>2</sub> sensor foil. (a) Sum image showing the PLIM imager field of view. (b-e) images of the area indicated in (a) centroided with different methods: (b) sum, (c) brightest pixel (BP), (d) earliest timecode, (e) centre-of-mass with 1/5 pixel accuracy (CoM 5). (f) Cross-sections of the bars in the area indicated in (e), where the sub-pixel centroiding can still resolve lines with ~40 μm spacing, that cannot be resolved with the other centroiding methods.

### 3.3 INSTRUMENT RESPONSE

To measure the instrument response function (IRF), the sensing film, which also contained a short-lived

aza-Bodipy dye, was imaged with the Tpx3Cam system. This dye is excitable with the same red LED (Figure 3f) as used for all measurements here showing fluorescence at 650 nm with lifetime in the low ns range<sup>43</sup>. The LED bias voltage was set to 4.0 V and the pulse duration to 50 ns, a minimum providing stable lifetime signal in Tpx3Cam.

Figure 6 shows several distributions of the photon arrival time with respect to the synchronous pulse received by the camera. Variation of this time provides information about the IRF. The time distributions for all hit pixels and for the centroided pixels are shown before and after the TOT correction. For the most inclusive measurement, all hit pixels were included, whereas for the centroided data only the earliest timecode for each photon hit was included, which explains different population of the histograms. The gaussian fit of the centroided, TOT corrected distribution has FWHM of 30.6 ns. The background was accounted for as a constant in the fit.

As expected, the centroiding significantly improves the temporal resolution of the Tpx3Cam imager by effectively selecting pixels with higher TOT which substantially reduces the timewalk effect. To account for the timewalk and to further improve the time resolution we apply the TOT correction by shifting the pixel TOA by an amount determined through a special calibration procedure<sup>46</sup>.

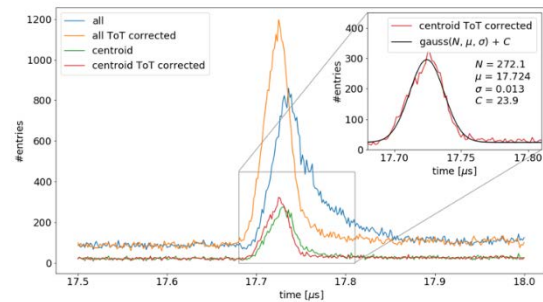


Figure 6. Instrument Resolution Function (IRF) position in the measurement time interval is shown for all hit pixels and for the centroided pixels. In both cases the distributions are shown before and after the TOT correction. Gaussian fit of the centroided and TOT corrected distribution corresponds to the IRF FWHM of 30.6 ns. Background was described with a constant in the fit.

To further illustrate effects of centroiding and TOT correction on the achievable timing resolution, Figure 7 presents the two-dimensional distributions of measured time versus TOT for four cases: (a) all hit pixels; (b) all hit pixels with TOT correction applied; (c) centroided pixels; (d) centroided pixels with TOT correction applied. We note that the non-centroided distribution is the most affected one by the timewalk as it contains many pixels with small signal. After the TOT correction the distributions are vertically oriented minimizing the time spread.

We note that the time resolution for this setup is dominated by the timing properties of the LED flash, which has a finite rise time and considerable 50 ns

duration and, thus, cannot be considered instantaneous. The FWHM resolution, 30.6 ns, achieved in the measurements is, therefore, limited by the LED and, no doubt, can be improved with more sophisticated illumination schemes. The time resolution for single photons measured in the experiments employing pairs of simultaneously produced entangled photons was measured to be better than FWHM 5.0 ns<sup>47</sup>.

Despite not exploiting fully the Tpx3Cam time resolution, the currently achieved IRF is adequate for PLIM applications with decay times in excess of 100 ns such, such as described below, and it will not limit the precision of lifetime measurements in this study.

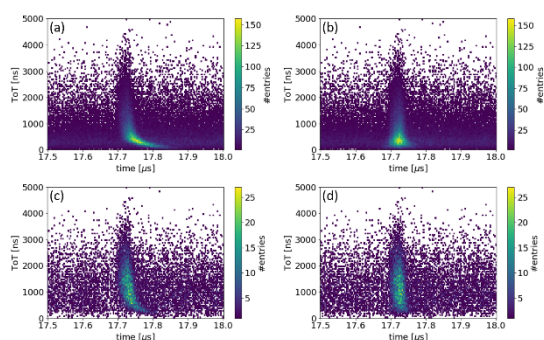


Figure 7. Two-dimensional distributions of time, in microseconds, versus TOT, in nanoseconds, for four cases: (a) all hit pixels; (b) all hit pixels with TOT correction applied; (c) centroided pixels; (d) centroided pixels with TOT correction applied.

### 3.4 PLIM IMAGING

Following the above optimisation of PLIM settings and data processing algorithms, several different phosphorescent samples were imaged on the Tpx3Cam imager to assess its performance. Excitation parameters (LED pulse width and amplitude) for each sample were optimised by observing the rate of photon events from the Tpx3Cam employing the on-line monitoring of frames in Sophy. To generate PLIM images, data from the camera was then collected for 20s for each sample. During the measurement of the solid state O<sub>2</sub> sensor, a total of 98,884 “frames” with 81 million triggered pixels were acquired at a pixel readout rate of 4 MHz. 12 million photon events were found in the event size range of 3-15 pixels and 0.7 million undersize and 2 million oversize events were discarded. This corresponds to accepted photon event count rate of ~0.6 MHz. Whereas, for the respiring HCT116 cells, 100,140 “frames” with 59 million triggered pixels were acquired at a pixel readout rate of 3 MHz. 10 million photon events were found in the size range of 3-15 pixels corresponding to a photon event count rate of ~0.5 MHz.

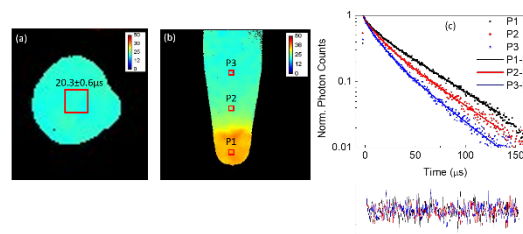


Figure 8. PLIM images obtained with Timepix3 imager: (a) PtBP-RL100 based O<sub>2</sub> sensor spotted on porous PVDF membrane; (b) Lifetime gradient caused by varying O<sub>2</sub> concentration in a tube with respiring HCT116 cells precipitated at the bottom; (c) Phosphorescent decays for areas marked in (b) with bi-exponential fits and residuals of fits.

Figure 8a shows PLIM image of a solid-state O<sub>2</sub>-sensitive coating, which was applied on a microporous membrane by spotting (see photograph on Figure 3d), measured in air (21% O<sub>2</sub>) at 24°C. One can see good homogeneity of phosphorescence lifetime within the spotted sensor, with mean lifetime values of 20.3 μs and standard deviation of 0.6 μs for the selected FoV (red box). The minute variations of lifetime values across the spot are due to the micro-heterogeneity of the sensor material. Such micro-heterogeneity is quite common for polymeric O<sub>2</sub> sensors, being comparable or even smaller for this example than for the other phosphorescent sensors imaged by confocal TCSPC-PLIM<sup>48</sup>.

In Figure 8b, the PLIM imager, together with the NanO<sub>2</sub>-IR probe added to the sample with live respiring cells, reveal the formation of a prominent O<sub>2</sub> gradient in the culturing tube. Probe lifetime values on the image are seen to largely increase towards the bottom of the tube, which reflects significant depletion of O<sub>2</sub> in this area due to the cell respiration<sup>49</sup>. Upon proper calibration of the probe, these lifetime values can be converted into O<sub>2</sub> concentration values and to the complete map of O<sub>2</sub> distribution within this biological sample<sup>11</sup>. Figure 8c shows the phosphorescent decay for the regions marked in Figure 8b and bi-exponential fits to the decays. The flat residuals indicate that a bi-exponential decay function provides a good fit to the decay. The fits yield decay times of 42.8 μs, 35.4 μs and 29.6 μs for P1, P2 and P3, with chi-squared values of 1.08, 1.01 and 1.03 respectively.

## 4. CONCLUSIONS

The Tpx3Cam coupled by means of Cricket@ adaptor with image intensifier, emission filter and macro-lens produced a compact and flexible PLIM imager. The spatial resolution of the system was assessed and optimised using different algorithms of centroiding of photon hit events. The resolving power was found to be 12.7 lp/mm, and line width - 39.4 μm. The IRF was also measured, which gave a temporal resolution of the system of 30.6 ns (FWHM).

The Tpx3Cam imager was then tested by imaging phosphorescent chemical and biological samples,

including a solid-state O<sub>2</sub> sensitive coating and a suspension of live mammalian cells in a test tube. Rather uniform lifetime distribution was obtained for the O<sub>2</sub> sensitive coating, whereas a prominent lifetime (i.e. O<sub>2</sub> concentration) gradient was revealed for the sample with respiring cells.

Overall, the new system shows good performance in PLIM mode, and is much faster than the other similar devices described previously. It can image objects of several centimetres in size with high spatial resolution and flexible optical alignment (e.g. vertical or horizontal configuration). In its present form, the imager is well-suited for various applications based on wide-field PLIM. System performance can be further improved and extended by replacing the LED with a fast laser source, which can also enable the nanosecond FLIM mode.

## AUTHOR INFORMATION

### Corresponding Authors

Email: [d.papkovsky@ucc.ie](mailto:d.papkovsky@ucc.ie); [anomerotski@bnl.gov](mailto:anomerotski@bnl.gov)

### Author Contributions

†These authors contributed equally.

## ACKNOWLEDGEMENT

Financial support of this work by Science Foundation Ireland, grants SFI/12/RC/2276, SFI/12/RC/2276\_P2 and SFI/17/RC-PhD/3484, is gratefully acknowledged. Authors are grateful to Prof. Sergey M. Borisov from Graz University of Technology, Austria, for a sample of aza-Bodipy dye used this study.

## REFERENCES

- (1) Korczyński, J.; Włodarczyk, J. Fluorescence Lifetime Imaging Microscopy (FLIM) in Biological and Medical Research. *Postepy Biochem.* **2009**, *55* (4), 434–440.
- (2) Marcu, L. Fluorescence Lifetime Techniques in Medical Applications. *Ann. Biomed. Eng.* **2012**, *40* (2), 304–331.
- (3) Wang, Z.; Zheng, Y.; Zhao, D.; Zhao, Z.; Liu, L.; Pliss, A.; Zhu, F.; Liu, J.; Qu, J.; Luan, P. Applications of Fluorescence Lifetime Imaging in Clinical Medicine. *J. Innov. Opt. Health Sci.* **2018**, *11* (01), 1830001. <https://doi.org/10.1142/s179354581830001x>.
- (4) Veetil, J. V.; Jin, S.; Ye, K. Fluorescence Lifetime Imaging Microscopy of Intracellular Glucose Dynamics. SAGE Publications 2012.
- (5) Agronskaia, A. V.; Tertoolen, L.; Gerritsen, H. C. Fast Fluorescence Lifetime Imaging of Calcium in Living Cells. *J. Biomed. Opt.* **2004**, *9* (6), 1230. <https://doi.org/10.1117/1.1806472>.
- (6) Lakowicz, J. R.; Szmajcinski, H.; Nowaczyk, K.; Johnson, M. L. Fluorescence Lifetime Imaging of Calcium Using Quin-2. *Cell Calcium* **1992**, *13* (3), 131–147.
- (7) Zheng, K.; Jensen, T. P.; Rusakov, D. A. Monitoring Intracellular Nanomolar Calcium Using Fluorescence Lifetime Imaging. *Nat. Protoc.* **2018**, *13* (3), 581–597. <https://doi.org/10.1038/nprot.2017.154>.
- (8) Orte, A.; Alvarez-Pez, J. M.; Ruedas-Rama, M. J. Fluorescence Lifetime Imaging Microscopy for the Detection of Intracellular PH with Quantum Dot

Nanosensors. *ACS Nano* **2013**, *7* (7), 6387–6395. <https://doi.org/10.1021/nn402581q>.

- (9) Lin, H.-J.; Herman, P.; Lakowicz, J. R. Fluorescence Lifetime-Resolved PH Imaging of Living Cells. *Cytometry* **2003**, *52A* (2), 77–89. <https://doi.org/10.1002/cyto.a.10028>.

- (10) Jenkins, J.; Dmitriev, R. I.; Papkovsky, D. B. Imaging Cell and Tissue O<sub>2</sub> by TCSPC-PLIM. In *Advanced Time-Correlated Single Photon Counting Applications*; Springer, 2015; pp 225–247.

- (11) Dmitriev, R. I.; Papkovsky, D. B. Optical Probes and Techniques for O<sub>2</sub> Measurement in Live Cells and Tissue. *Cell. Mol. life Sci.* **2012**, *69* (12), 2025–2039.

- (12) Kalinina, S.; Schaefer, P.; Breyer, J.; Bisinger, D.; Chakraborty, S.; Rueck, A. Oxygen Sensing PLIM Together with FLIM of Intrinsic Cellular Fluorophores for Metabolic Mapping. In *Imaging, Manipulation, and Analysis of Biomolecules, Cells, and Tissues XVI*; International Society for Optics and Photonics, 2018; Vol. 10497, p 104970F.

- (13) Kavandi, J.; Callis, J.; Gouterman, M.; Khalil, G.; Wright, D.; Green, E.; Burns, D.; McLachlan, B. Luminescent Barometry in Wind Tunnels. *Rev. Sci. Instrum.* **1990**, *61* (11), 3340–3347. <https://doi.org/10.1063/1.1141632>.

- (14) Seidenari, S.; Arginelli, F.; Bassoli, S.; Cautela, J.; French, P. M. W.; Guanti, M.; Guardoli, D.; König, K.; Talbot, C.; Dunsby, C. Multiphoton Laser Microscopy and Fluorescence Lifetime Imaging for the Evaluation of the Skin. *Dermatol. Res. Pract.* **2012**, *2012*, 1–9. <https://doi.org/10.1155/2012/810749>.

- (15) Dysli, C.; Wolf, S.; Berezin, M. Y.; Sauer, L.; Hammer, M.; Zinkernagel, M. S. Fluorescence Lifetime Imaging Ophthalmoscopy. *Prog. Retin. Eye Res.* **2017**, *60*, 120–143. <https://doi.org/10.1016/j.preteyeres.2017.06.005>.

- (16) Sharick, J. T.; Jeffery, J. J.; Karim, M. R.; Walsh, C. M.; Esbona, K.; Cook, R. S.; Skala, M. C. Cellular Metabolic Heterogeneity In Vivo Is Recapitulated in Tumor Organoids. *Neoplasia (United States)* **2019**, *21* (6), 615–626. <https://doi.org/10.1016/j.neo.2019.04.004>.

- (17) Becker, W. Fluorescence Lifetime Imaging - Techniques and Applications. *J. Microsc.* **2012**, *247* (2), 119–136. <https://doi.org/10.1111/j.1365-2818.2012.03618.x>.

- (18) Becker, W. 3 Advanced TCSPC-FLIM Techniques. **2018**.

- (19) Wei, L.; Yan, W.; Ho, D. Recent Advances in Fluorescence Lifetime Analytical Microsystems: Contact Optics and CMOS Time-Resolved Electronics. *Sensors (Switzerland)* **2017**, *17* (12), 2800. <https://doi.org/10.3390/s17122800>.

- (20) Hirvonen, L. M.; Suhling, K. Wide-Field TCSPC: Methods and Applications. *Meas. Sci. Technol.* **2017**, *28* (1), 012003. <https://doi.org/10.1088/1361-6501/28/1/012003>.

- (21) Sparks, H.; Görlitz, F.; Kelly, D. J.; Warren, S. C.; Kellett, P. A.; Garcia, E.; Dymoke-Bradshaw, A. K. L.; Hares, J. D.; Neil, M. A. A.; Dunsby, C.; et al. Characterisation of New Gated Optical Image Intensifiers for Fluorescence Lifetime Imaging. *Rev. Sci. Instrum.* **2017**, *88* (1), 012003.

- (22) Hirvonen, L. M.; Festy, F.; Suhling, K. Wide-Field Time-Correlated Single-Photon Counting (TCSPC) Lifetime Microscopy with Microsecond Time Resolution. *Opt. Lett.* **2014**, *39* (19), 5602. <https://doi.org/10.1364/ol.39.005602>.

- (23) Petrášek, Z.; Suhling, K. Photon Arrival Timing with Sub-Camera Exposure Time Resolution in Wide-Field Time-Resolved Photon Counting Imaging. *Opt. Express* **2010**, *18* (24), 24888. <https://doi.org/10.1364/oe.18.024888>.

- (24) Hirvonen, L. M.; Petrášek, Z.; Beeby, A.; Suhling, K. Sub-Ms Time Resolution in Wide-Field Time-Correlated Single Photon Counting Microscopy Obtained

- from the Photon Event Phosphor Decay. *New J. Phys.* **2015**, *17*, 023032. <https://doi.org/10.1088/1367-2630/17/2/023032>.
- (25) Gersbach, M.; Trimananda, R.; Maruyama, Y.; Fishburn, M.; Stoppa, D.; Richardson, J.; Walker, R.; Henderson, R. K.; Charbon, E. High Frame-Rate TCSPC-FLIM Using a Novel SPAD-Based Image Sensor. *Detect. Imaging Devices Infrared, Focal Plane, Single Phot.* **2010**, *7780* (May 2014), 77801H. <https://doi.org/10.1117/12.860769>.
- (26) Fisher-Levine, M.; Nomerotski, A. TimepixCam: A Fast Optical Imager with Time-Stamping. *J. Instrum.* **2016**, *11* (3), C03016. <https://doi.org/10.1088/1748-0221/11/03/C03016>.
- (27) Nomerotski, A. Imaging and Time Stamping of Photons with Nanosecond Resolution in Timepix Based Optical Cameras. *Nucl. Instruments Methods Phys. Res. Sect. A Accel. Spectrometers, Detect. Assoc. Equip.* **2019**, *937*, 26–30. <https://doi.org/10.1016/j.nima.2019.05.034>.
- (28) Llopart, X.; Ballabriga, R.; Campbell, M.; Tlustos, L.; Wong, W. Erratum to “Timepix, a 65 k Programmable Pixel Readout Chip for Arrival Time, Energy and/or Photon Counting Measurements” [Nucl. Instr. and Meth. A. 581 (2007) 485–494] (DOI:10.1016/j.Nima.2007.08.079). *Nucl. Instruments Methods Phys. Res. Sect. A Accel. Spectrometers, Detect. Assoc. Equip.* **2008**, *585* (1–2), 106–108. <https://doi.org/10.1016/j.nima.2007.11.003>.
- (29) Nomerotski, A.; Chakaberia, I.; Fisher-Levine, M.; Janoska, Z.; Takacs, P.; Tsang, T. Characterization of TimepixCam, a Fast Imager for the Time-Stamping of Optical Photons. *J. Instrum.* **2017**, *12* (1), C01017. <https://doi.org/10.1088/1748-0221/12/01/C01017>.
- (30) Hirvonen, L. M.; Fisher-Levine, M.; Suhling, K.; Nomerotski, A. Photon Counting Phosphorescence Lifetime Imaging with TimepixCam. *Rev. Sci. Instrum.* **2017**, *88* (1), 013104. <https://doi.org/10.1063/1.4973717>.
- (31) Poikela, T.; Plosila, J.; Westerlund, T.; Campbell, M.; Gaspari, M. De; Llopart, X.; Gromov, V.; Kluit, R.; Beuzekom, M. Van; Zappone, F.; et al. Timepix3: A 65K Channel Hybrid Pixel Readout Chip with Simultaneous ToA/ToT and Sparse Readout. *J. Instrum.* **2014**, *9* (5), C05013. <https://doi.org/10.1088/1748-0221/9/05/C05013>.
- (32) Visser, J.; Beuzekom, M. Van; Boterenbrood, H.; Heijden, B. Van Der; Muñoz, J. I.; Kulis, S.; Munneke, B.; Schreuder, F. SPIDR: A Read-out System for Medipix3 & Timepix3. *J. Instrum.* **2015**, *10* (12), C12028. <https://doi.org/10.1088/1748-0221/10/12/C12028>.
- (33) Al Darwish, R.; Marcu, L.; Bezak, E. Overview of Current Applications of the Timepix Detector in Spectroscopy, Radiation and Medical Physics. *Appl. Spectrosc. Rev.* **2019**, 1–19.
- (34) Beacham, R.; Mac Raighne, A.; Maneuski, D.; O’Shea, V.; McVitie, S.; McGrouther, D. Medipix2/Timepix Detector for Time Resolved Transmission Electron Microscopy. *J. Instrum.* **2011**, *6* (12), C12052. <https://doi.org/10.1088/1748-0221/6/12/C12052>.
- (35) Procz, S.; Avila, C. A.; Fey, J.; Roque, G. A.; Schuetz, M.; Hamann, E. X-Ray and Gamma Imaging with Medipix and Timepix Detectors in Medical Research. *Radiat. Meas.* **2019**, Vol. 127, 106104. <https://doi.org/10.1016/j.radmeas.2019.04.007>.
- (36) Fisher-Levine, M.; Boll, R.; Ziaee, F.; Bomme, C.; Erk, B.; Rompotis, D.; Marchenko, T.; Nomerotski, A.; Rolles, D. Time-Resolved Ion Imaging at Free-Electron Lasers Using TimepixCam. *J. Synchrotron Radiat.* **2018**, *25* (2), 336–345.
- (37) Chelushkin, P. S.; Tunik, S. P. *Progress in Photon Science*; Springer International Publishing, 2017; Vol. 115. <https://doi.org/10.1007/978-3-319-52431-3>.
- (38) Zarychta-Wisniewska, W.; Burdzinska, A.; Zagodzón, R.; Dybowski, B.; Butrym, M.; Gajewski, Z.; Paczek, L. In Vivo Imaging System for Explants Analysis—A New Approach for Assessment of Cell Transplantation Effects in Large Animal Models. *PLoS One* **2017**, *12* (9), 1–21. <https://doi.org/10.1371/journal.pone.0184588>.
- (39) Photonis Cricket: <https://www.photonis.com/products/cricket>.
- (40) Barber, P. R.; Ameer-Beg, S. M.; Gilbey, J.; Carlin, L. M.; Keppler, M.; Ng, T. C.; Vojnovic, B. Multiphoton Time-Domain Fluorescence Lifetime Imaging Microscopy: Practical Application to Protein-Protein Interactions Using Global Analysis. *J. R. Soc. Interface* **2009**, *6* (ISSUE SUPPL. 1). <https://doi.org/10.1098/rsif.2008.0451.focus>.
- (41) Tsytsarev, V.; Akkenti, F.; Pumbo, E.; Tang, Q.; Chen, Y.; Erzurumlu, R. S.; Papkovsky, D. B. Planar Implantable Sensor for in Vivo Measurement of Cellular Oxygen Metabolism in Brain Tissue. *J. Neurosci. Methods* **2017**, *281*, 1–6. <https://doi.org/10.1016/j.jneumeth.2017.02.005>.
- (42) Lu, H.; MacK, J.; Yang, Y.; Shen, Z. Structural Modification Strategies for the Rational Design of Red/NIR Region BODIPYs. *Chem. Soc. Rev.* **2014**, *43* (13), 4778–4823. <https://doi.org/10.1039/c4cs00030g>.
- (43) Jokic, T.; Borisov, S. M.; Saf, R.; Nielsen, D. A.; Kühl, M.; Klimant, I. Highly Photostable Near-Infrared Fluorescent PH Indicators and Sensors Based on BF<sub>2</sub>-Chelated Tetraarylazadipyrromethene Dyes. *Anal. Chem.* **2012**, *84* (15), 6723–6730. <https://doi.org/10.1021/ac3011796>.
- (44) Tsytsarev, V.; Arakawa, H.; Borisov, S.; Pumbo, E.; Erzurumlu, R. S.; Papkovsky, D. B. In Vivo Imaging of Brain Metabolism Activity Using a Phosphorescent Oxygen-Sensitive Probe. *J. Neurosci. Methods* **2013**, *216* (2), 146–151. <https://doi.org/10.1016/j.jneumeth.2013.04.005>.
- (45) Zhao, A.; Van Beuzekom, M.; Bouwens, B.; Byelov, D.; Chakaberia, I.; Cheng, C.; Maddox, E.; Nomerotski, A.; Svihra, P.; Visser, J.; et al. Coincidence Velocity Map Imaging Using Tpx3Cam, a Time Stamping Optical Camera with 1.5 Ns Timing Resolution. *Rev. Sci. Instrum.* **2017**, *88* (11), 113104. <https://doi.org/10.1063/1.4996888>.
- (46) Tsigaridas, S.; Beuzekom, M. V.; Graaf, H. V.D.; Hartjes, F.; Heijhoff, K.; Hesse, N. P.; de Jong, P. J.; Prodanovic, V. Timewalk Correction for the Timepix3 Chip Obtained with Real Particle Data. *Nucl. Instruments Methods Phys. Res. Sect. A Accel. Spectrometers, Detect. Assoc. Equip.* **2019**, *930*, 185–190. <https://doi.org/10.1016/j.nima.2019.03.077>.
- (47) Ianzano, C.; Svihra, P.; Flament, M.; Hardy, A.; Cui, G.; Nomerotski, A.; Figueroa, E. Spatial Characterization of Photonic Polarization Entanglement Using a Tpx3Cam Intensified Fast-Camera. **2018**, 1–22.
- (48) Kelly, C. A.; Toncelli, C.; Kerry, J. P.; Papkovsky, D. B. Discrete O<sub>2</sub> Sensors Produced by a Spotting Method on Polyolefin Fabric Substrates. *Sensors Actuators B Chem.* **2014**, *203*, 935–940.
- (49) Zhdanov, A. V.; Ogurtsov, V. I.; Taylor, C. T.; Papkovsky, D. B. Monitoring of Cell Oxygenation and Responses to Metabolic Stimulation by Intracellular Oxygen Sensing Technique. *Integr. Biol.* **2010**, *2* (9), 443–451.

# TOC Graphic

---

